AGU PUBLICATIONS

JGR

Journal of Geophysical Research: Oceans

RESEARCH ARTICLE

10.1002/2017JC012956

Special Section:
Oceanic Responses and Feedbacks to Tropical Cyclones

Impact of Langmuir Turbulence on Upper Ocean Response to Hurricane Edouard: Model and Observations

A. Blair[1], I. Ginis[1], T. Hara[1], and E. Ulhorn[2]

[1]Graduate School of Oceanography, University of Rhode Island, Narragansett, RI, USA, [2]AIR-Worldwide, Boston, MA, USA

Abstract Tropical cyclone intensity is strongly affected by the air-sea heat flux beneath the storm. When strong storm winds enhance upper ocean turbulent mixing and entrainment of colder water from below the thermocline, the resulting sea surface temperature cooling may reduce the heat flux to the storm and weaken the storm. Recent studies suggest that this upper ocean turbulence is strongly affected by different sea states (Langmuir turbulence), which are highly complex and variable in tropical cyclone conditions. In this study, the upper ocean response under Hurricane Edouard (2014) is investigated using a coupled ocean-wave model with and without an explicit sea state dependent Langmuir turbulence parameterization. The results are compared with in situ observations of sea surface temperature and mixed layer depth from AXBTs, as well as satellite sea surface temperature observations. Overall, the model results of mixed layer deepening and sea surface temperature cooling under and behind the storm are consistent with observations. The model results show that the effects of sea state dependent Langmuir turbulence can be significant, particularly on the mixed layer depth evolution. Although available observations are not sufficient to confirm such effects, some observed trends suggest that the sea state dependent parameterization might be more accurate than the traditional (sea state independent) parameterization.

Key Points:
- Accurate predictions of upper ocean response to a tropical cyclone requires a sea-state dependent Langmuir turbulence parameterization
- The model simulations of upper ocean response under Hurricane Edouard are consistent with in situ observations
- Some observed trends suggest that the sea-state dependent Langmuir turbulence parameterization might be more accurate

Correspondence to:
A. Blair,
a_blair@uri.edu

Citation:
Blair, A., Ginis, I., Hara, T., & Ulhorn, E. (2017). Impact of Langmuir turbulence on upper ocean response to Hurricane Edouard: Model and observations. *Journal of Geophysical Research: Oceans*, *122*, 9712–9724. https://doi.org/10.1002/2017JC012956

Received 2 APR 2017
Accepted 15 NOV 2017
Accepted article online 17 NOV 2017
Published online 10 DEC 2017

1. Introduction

The air-sea heat flux is a primary constraint on the energy budget of a tropical cyclone (Emanuel, 1991). Tropical cyclones (TC) rely on the transfer of latent heat energy from the upper ocean to the atmosphere for formation and maintenance of intensity. Even minor changes in sea surface temperature (SST) can result in significant changes to storm intensity, as the latent heat flux is very sensitive to the temperature difference between surface waters and adjacent air (Bender & Ginis, 2000; Ginis, 2002). The large wind stress applied to the ocean by the TC often reduces the SST by enhancing upper ocean vertical turbulent mixing, entraining colder water from below the thermocline, and deepening the mixed layer. Therefore, in order to accurately predict TC intensity, it is essential to couple an ocean model to the atmospheric model to obtain an SST forecast (D'Asaro et al. 2014; Jaimes et al. 2015; Lin et al. 2013). Furthermore, three-dimensional ocean models have been shown to improve predictions of intensity when coupled (Bender et al. 2007; Ginis, 2002; Schade & Emanuel, 1999), whereas one-dimensional models may not properly represent the spatial variability and intensity of the upper ocean cooling (Yablonsky & Ginis, 2009). Realistic initialization of the temperature field within the ocean model is also critical to properly predict SST cooling (Halliwell et al., 2008; Yablonsky et al. 2015b)

The simulated response of the upper ocean to TCs is also dependent on accurate wind forcing (wind stress) fields and proper parameterizations of turbulent mixing, and recent research indicates that sea-state (surface wave conditions) can significantly modify both. These wave impacts are particularly influential under TCs where the sea-state is spatially and temporally complex. Therefore, a wave model must be coupled to the TC-ocean model to properly account for these sea-state effects. Growing or decaying wave fields absorb or release momentum and modify the momentum flux into upper ocean relative to the wind stress (Fan et al., 2010; Smith, 2006). This effect is often called the "air-sea momentum flux budget." Ocean surface wave fields also affect vertical turbulent mixing because the upper ocean turbulence is modified by the Stoke drift of the waves, known as Langmuir turbulence (LT). The sea state dependent LT under TCs has been studied extensively using large eddy simulations (Rabe et al., 2015; Reichl et al., 2016a; Sullivan et al. 2012). The latter study has developed a mixing scheme that accurately parameterizes the LT under a wide range of sea states under TCs, by modifying the existing k-profile parameterization (KPP). Reichl et al.

(2016b) has introduced this modified LT mixing scheme to a coupled ocean–wave model, and has shown that the three-dimensional upper ocean response and sea surface temperature cooling may be significantly modified by the sea state dependence of the LT under idealized TC wind forcing.

This study will apply the same explicitly sea-state dependent LT mixing scheme to the upper ocean numerical simulation under Hurricane Edouard, a storm that occurred over the Atlantic Ocean in September 2014. Two additional mixing schemes that are independent of sea state are also applied for comparison. The National Oceanic and Atmospheric Administration Hurricane Research Division (NOAA-HRD) conducted an extensive field campaign, before, during and after Hurricane Edouard, providing valuable in situ observations. These in situ observations, as well as satellite observations of the SST, allow for a comparison of the model results to observations throughout the surface water column to evaluate the model performance and the LT impact.

2. Field Observations and Methods

2.1. Hurricane Edouard Observations

A tropical depression strengthened into Tropical Storm Edouard on 12 September 2014 (Stewart, 2014). As part of a NOAA Hurricane Research Division (HRD) air-sea interaction study, WP-3D aircraft dropped an initial series of Airborne Expendable Bathy Thermographs (AXBTs) in the projected path of the storm (Figure 1). Further deployments of AXBTs were conducted on the 14th, 15th, and 16th on flight paths through the center of the storm as it traveled through the region. The storm was classified as a hurricane on the 14th, and reached major hurricane (winds greater than 178 km/h) status for a short time on the 16th before weakening and returning to standard hurricane status until 18 September. A final series of AXBT drops was conducted on the 17th closely following the locations of the initial 12 September drops, after Edouard had left the region. A total of 84 AXBT temperature profiles from these flights are used in this study (Figure 2). The AXBTs typically provided data to at least 350m depth.

Additional SST data were obtained using the IRsonde during the same field program (Zhang et al., 2017). Comparisons between SSTs measured by collocated IRsondes and AXBTs show good agreement, especially in regions with no rain contamination. Since the AXBT measures the water side temperature more directly, the IRsondes SST data are not used for model comparison in this study.

The satellite SST data used in this study are daily Microwave OI SST fields produced by Remote Sensing Systems and sponsored by National Oceanographic Partnership Program (NOPP) and the NASA Earth Science Physical Oceanography Program. Using the TMI, AMSR-E, AMSR2 and WindSat satellites, the data are optimally interpolated to create a gridded field. Data are available at www.remss.com/measurements/sea-surface-temperature. It is worth noting that during Hurricane Edouard measurements of the air temperature, moisture, and winds, were made at $\sim$760 m altitude using the Coyote UAS platform for the first time (Cione et al., 2016). In the future, Coyote hurricane missions will also utilize a downward-looking infrared sensor that will be capable of measuring sea surface temperature. These measurements will help to validate ocean model simulated SSTs right underneath the hurricane.

2.2. Model Description

The model experiments were conducted using a standalone ocean model or an ocean model coupled with a wave model. The model was forced using the atmospheric parameters data set for Edouard, also known as the TC vitals (Trahan & Sparling, 2012), which includes six-hourly storm center positions, maximum wind speeds, radii of maximum wind and outermost closed isobar, radii of 17, 26, and 33 m s^{-1} winds in the northeast, southeast, southwest, and northwest quadrants of the storm, and central and environmental pressure. The TC vitals maximum wind compares well to the National Hurricane Center (NHC) official Best Track report for Edouard (Figure 3). The surface wind distribution is based on interpolation of the radial wind profiles derived from the TC vitals (Yablonsky et al., 2015b). Examples of the wind fields on 13–17 September at 0000 UTC are shown in Figure 1.

The wave model used in the coupled model system is WAVEWATCH III (WW3) version 3.14. WW3 is a 3rd generation wave model that solves the spectral action density balance equation for wavenumber-direction spectra (Tolman, 2009). Starting at a minimum frequency of 0.0285 Hz, the wave spectrum is calculated at 40 logarithmically spaced intervals. Twenty-four discrete wave direction are used, ranging from 0 to 2π in

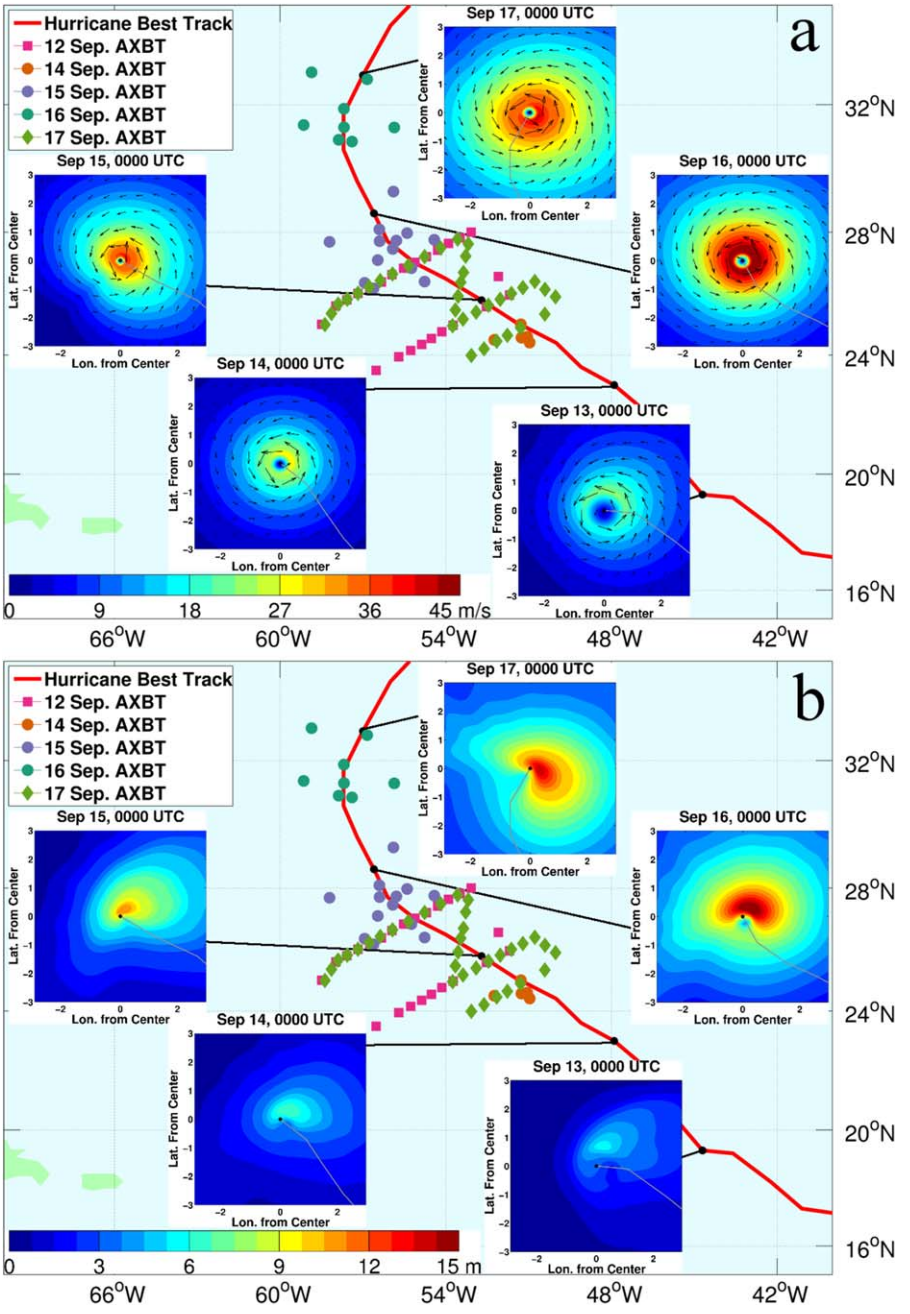

Figure 1. Modeled Tropical Cyclone Edouard parameters at 0000 UTC on five consecutive days from 13 to 17 September along the storm best track, with AXBT drop locations shown (colored symbols). (a) Model wind fields based on TC vitals, applied to all model simulations. (b) Modeled significant wave heights.

$\pi/12$ increments. The modeled significant wave heights on 13–17 September at 0000 UTC are shown in Figure 1.

The ocean model (either standalone or coupled with the wave model) is MPIPOM-TC (Yablonsky et al., 2015a), an updated version of the Princeton Ocean Model (POM; Blumberg & Mellor, 1987; Mellor, 2004) modified to use parallel processing. MPIPOM-TC is a three-dimensional primitive equation numerical model, in which horizontal differencing scheme calculations are performed on an Arakawa C-grid with curvilinear coordinates. The model domain covers −98.5° E to −15.3° E longitudinally, and 10° N to 47.5° N latitudinally, with a horizontal grid spacing of 1/12°. A realistic topography is used, with vertical coordinates of 60

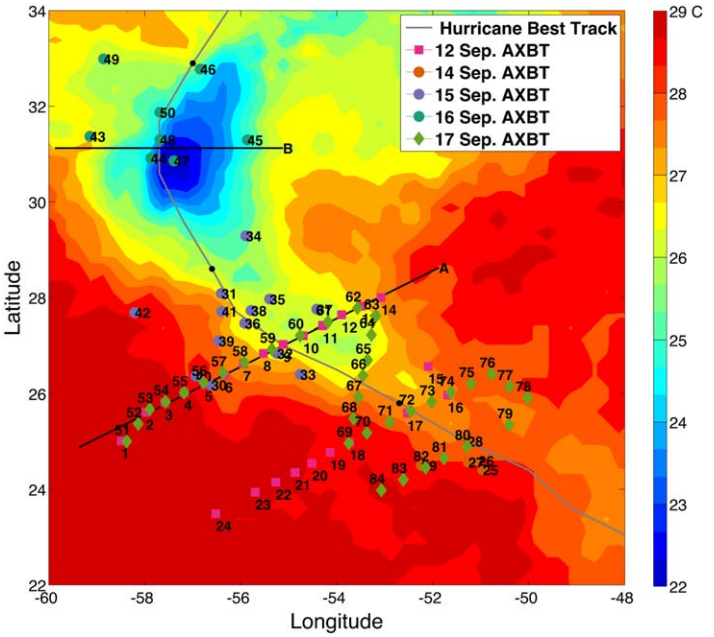

Figure 2. Numbered AXBT drop locations on a background of satellite observed SST on 17 September 0000 UTC. Two thick black lines denote two virtual transects used in this study.

depth scaled sigma levels. Compared to the original 23 sigma layers in MPIPOM, 60 layers allows for finer resolution within and below the mixing layer (Figure 4).

The classic Mellor-Yamada vertical mixing scheme (Mellor & Yamada, 1982) typically used in POM has been replaced by the K Profile Parameterization scheme (KPP) of Large et al. (1994). Three configurations of the KPP mixing scheme are used, in a manner identical to those in Reichl et al. (2016a). The first, hereafter KPP, has no sea-state dependent effects and uses a critical Richardson number of 0.35 to simulate typical (sea state independent) LT. The second, KPP-ST, is tuned for shear turbulence only conditions (no LT) and the Critical Richardson number is set 0.27. KPP-ST has no sea-state dependent effects as well. Both KPP and KPP-ST are used in the standalone ocean model.

The third KPP configuration, KPP-LT, is used in the coupled ocean-wave model and simulates the sea state dependent LT. In KPP-LT, the critical Richardson number is set 0.27, as in KPP-ST, but additional sea-state dependent enhancements are added to the turbulence parameterization. Specifically, Lagrangian current shear and an enhanced (sea-state dependent) eddy viscosity are used in the turbulent momentum flux calculations, and the unresolved shear in the calculation of the bulk Richardson number is enhanced.

The original MPIPOM momentum equations, which are used in the standalone ocean model, are

$$\partial_t u_h + (\mathbf{u}\cdot\nabla)u_h + \varepsilon_{h3j} f u_j - D_h + \partial_h p = 0 \tag{2.1}$$

$$-b + \partial_z p = 0 \tag{2.2}$$

where $h=1,2; j=1,2,3$, (x,y) are the horizontal coordinates, z is the vertical coordinate, t is the time, ∇ denotes 3D gradient, b is the buoyancy, p is the pressure divided by the reference density, f is the Coriolis parameter, D_h is the turbulent diffusion, $\mathbf{u}=(u, v, w)$ is the (3D) Eulerian velocity. In the coupled ocean-wave model, we have replaced the Eulerian currents in the MPIPOM momentum equations by the Lagrangian currents. Our modifications begin with the work of Fox-Kemper and Suzuki (2016) who show that in the presence of surface waves equations (2.1) and (2.2) should be modified to

$$\partial_t u_h + (\mathbf{u}^L\cdot\nabla)u_h + \varepsilon_{h3j} f u^L_j - D_h + \partial_h p = -u^L_i \partial_h u^S_i \tag{2.3}$$

$$-b + \partial_z p = -u^L_i \partial_z u^S_i \tag{2.4}$$

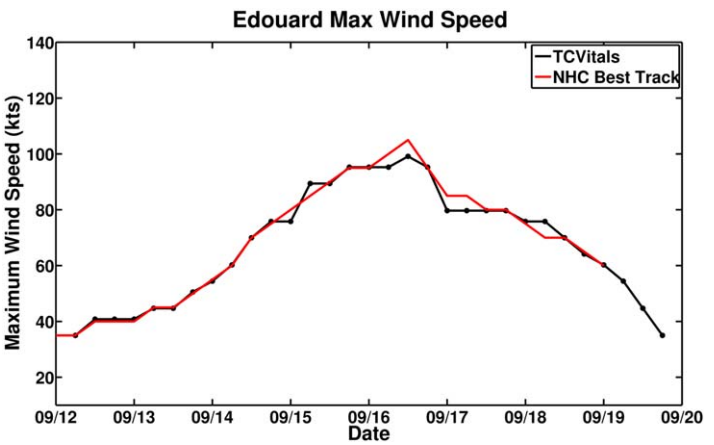

Figure 3. Maximum wind speed of Hurricane Edouard (in knots) from TC vitals (black line) and NHC Best Track (red line).

where all flow variables are now averaged over a short time to filter out the rapid oscillation of surface waves, $\boldsymbol{u}^S$ is the Stokes drift, and $\boldsymbol{u}^L=\mathbf{u}+\boldsymbol{u}^S$ is the Lagrangian velocity. The vertical component of the Stokes drift is added when the Stokes drift is horizontally divergent, to satisfy the continuity. The right-hand terms in (2.3) and (2.4) are called the Stokes shear force. The Stokes shear force is responsible for enhancing the turbulent mixing (Langmuir turbulence) in unresolved (subgrid) scales. Equation (2.3) can be rewritten as

$$\partial_t u^L_h + (\mathbf{u}^L\cdot\nabla)u^L_h + \varepsilon_{h3j} f u^L_j - D_h + \partial_h p = \partial_t u^S_h + (\mathbf{u}^L\cdot\nabla)u^S_h - u^L_i \partial_h u^S_i \tag{2.5}$$

where the left-hand terms are now the same as the left-hand terms of the original POM equation (equation (2.1)) if the Eulerian current is replaced by the Lagrangian current. The last two terms on the right side of equation (2.5) are typically negligibly small under TC conditions. We can therefore use the original MPIPOM-TC code to solve for the Lagrangian current simply by adding the term $\partial_t u^S_h$ to the

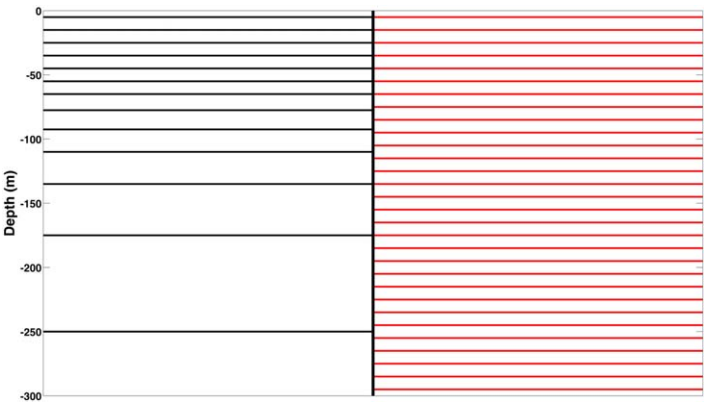

Figure 4. A comparison of the upper ocean model resolution in (left) the original POM (black) and (right) our modified MPIPOM-TC (red) models.

equation. In the presence of surface waves, the turbulent diffusion D_h is now parameterized in terms of the Lagrangian current shear, instead of the Eulerian current shear, and the scalar and continuity equations are also written in terms of the Lagrangian current instead of the Eulerian current.

The momentum equation (2.5) is forced by the wind stress τ_h applied at the surface. Therefore, if we integrate (2.5) in z from $-\infty$ to 0, the diffusion term D_h disappears but the right-hand side should include the surface forcing term τ_h. When the surface wave field is growing or decaying, Smith (2006) and Fan et al. (2010) show that the momentum flux into the upper ocean is modified from the direct wind stress by a difference of approximately

$$\nabla\tau_h = -\partial_t M_h - \nabla_i S_{hi} \tag{2.6}$$

where $M_h = \int_{-\infty}^{0} u_h^S(z)dz$ is the vertically integrated Stokes drift and S_{hi} is the vertically integrated radiation stress. The appropriate forcing on the ocean model is then $\tau_h + \nabla\tau_h$ instead of τ_h. The negative of the first term on the right of equation (2.6) is identical to the vertical integral of the first term of the right of equation (2.5); if we ignore the fact that the former applies at the surface and the latter applies through the water column, the two terms exactly cancel.

In summary, by removing the time dependent term $\partial_t M_h$ in the air-sea momentum flux budget calculation (2.6), the MPIPOM equation is not modified, but the current output of the model is interpreted as the Lagrangian current instead of the Eulerian current. Note that this approach does ignore the vertical Stokes shear force on the right-side of equation (2.4), which is left for investigation in future studies.

The ocean model is initialized using a Feature-Based (FB) method that begins by generating an initial three-dimensional ocean from the Generalized Digital Environmental Model (GDEM; Falkovich et al., 2005; Yablonsky & Ginis, 2008). This is a monthly temperature and salinity climatology (Teague et al., 1990) given at 0.5° horizontal grid spacing and 33 vertical z-levels which is interpolated spatially and temporally onto the MPIPOM grid at the chosen initial date. Since oceanic fronts and eddies are poorly represented in the GDEM climatology, a cross-frontal feature-based sharpening is performed to obtain more realistic fields. The feature-based modeling procedure allows one to initialize the Gulf Stream and eddies in the Atlantic basin based on guidance from real-time satellite altimetry. The upper ocean temperature is then modified by assimilating the real-time daily SST fields from the NOAA's operational Global Forecast System analysis (Reynolds & Smith, 1994). The ocean model is then spun up for two days for dynamical adjustment of the temperature and salinity fields and generation of ocean currents.

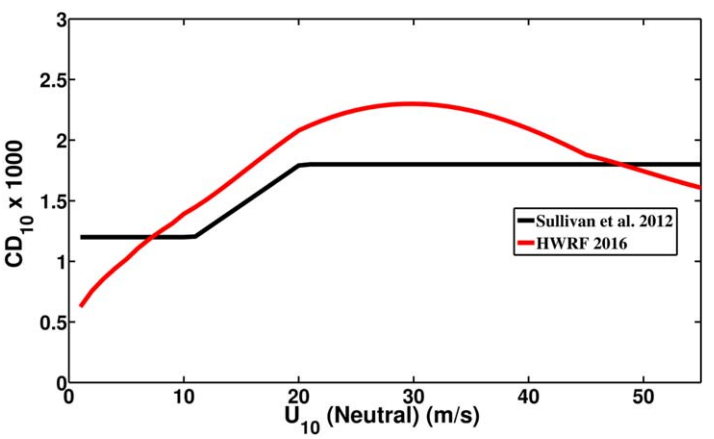

Figure 5. A comparison of the HWRF 2016 and Sullivan et al. (2012) drag parameterizations used in this study.

An investigation into the impacts of different drag coefficient parameterizations is also performed. The majority of the results shown in this study are from simulations using the 2016 Hurricane Weather Research and Forecasting (HWRF) model drag parameterization (Biswas et al., 2016), while all experiments have been repeated with a drag parameterization based on Sullivan et al. (2012) (Figure 5).

3. Comparison of Model Results to Observations

3.1. Evaluation of Initialization

On 12 September, before Hurricane Edouard entered the study region, the Feature-Based initialization of the ocean model SST shows a pool of water with temperatures of 29° or warmer extending east to west. The temperature field compares reasonably well with satellite observations from the 12th, mostly less than ± 1° C (Figure 6).

The pre-storm temperature field also agrees with the AXBT profiles available from 12 September mostly within ± 1° C (Figure 7a). Along

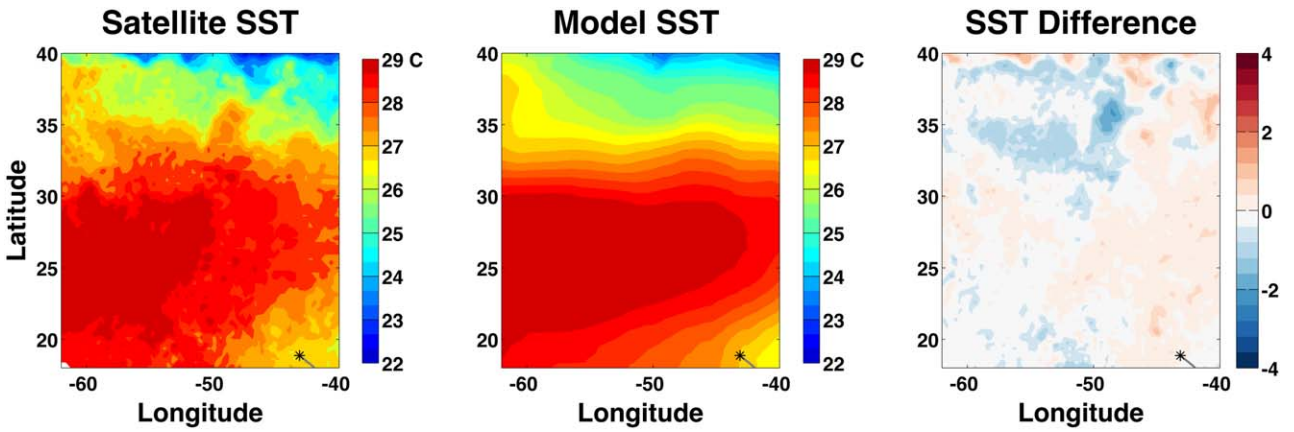

Figure 6. Comparison of (a) satellite observed SST to (b) initial MPIPOM SST on 12 September. The difference (model minus observation) is shown in (c). The black star marks the storm center at 12 September, 1600 UTC.

the Transect A (defined in Figure 2) the model SST has a somewhat positive bias to the AXBT profiles on the east end of transect, but agrees well with the satellite SST along the entire transect (Figure 7c).

A comparison of mixed layer depth (MLD), another characteristic of vertical temperature profiles important to TCs, can also be made using AXBT profiles. The model results agree well with the AXBT results, mostly within $\pm$ 10 m (Figures 7b and 7d). Here we define the MLD after Yablonsky and Ginis (2008) as the deepest layer where the difference between the temperature of that layer and the SST is $\leq$0.5° C. We first interpolate

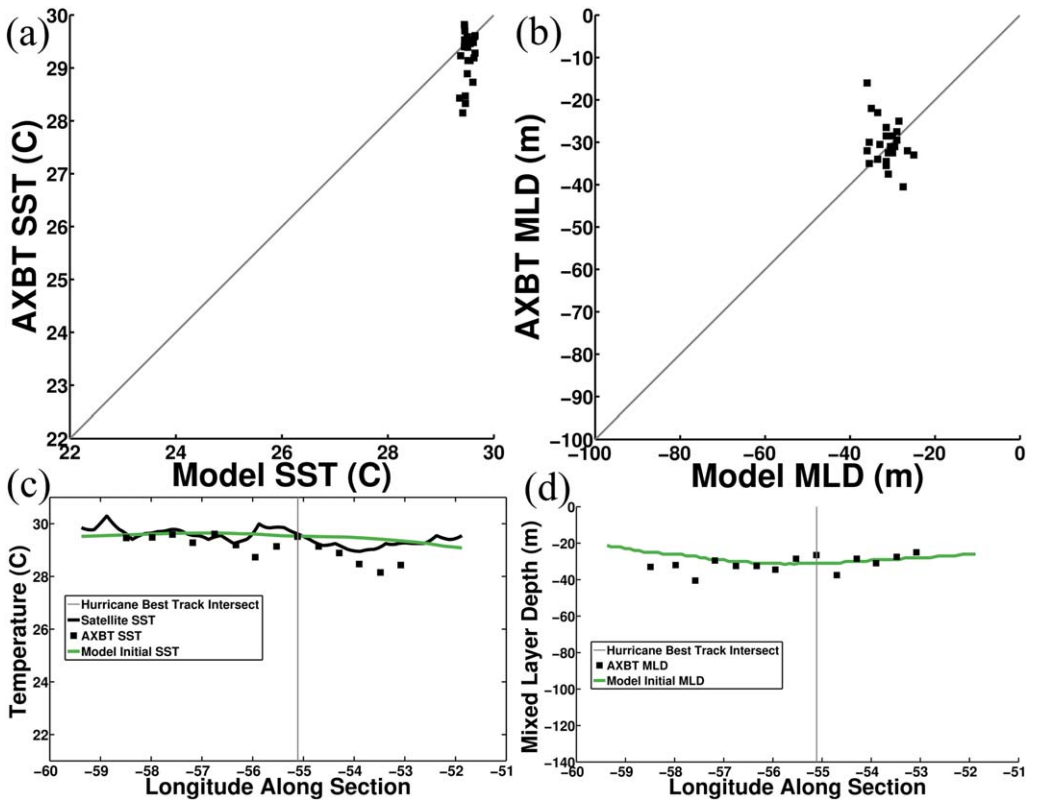

Figure 7. Comparisons between model and observations of SST and mixed layer depth at 12 September, 1600 UTC. (a) SST, (b) mixed layer depth, (c) SST along Transect A, (d) mixed layer depth along Transect A.

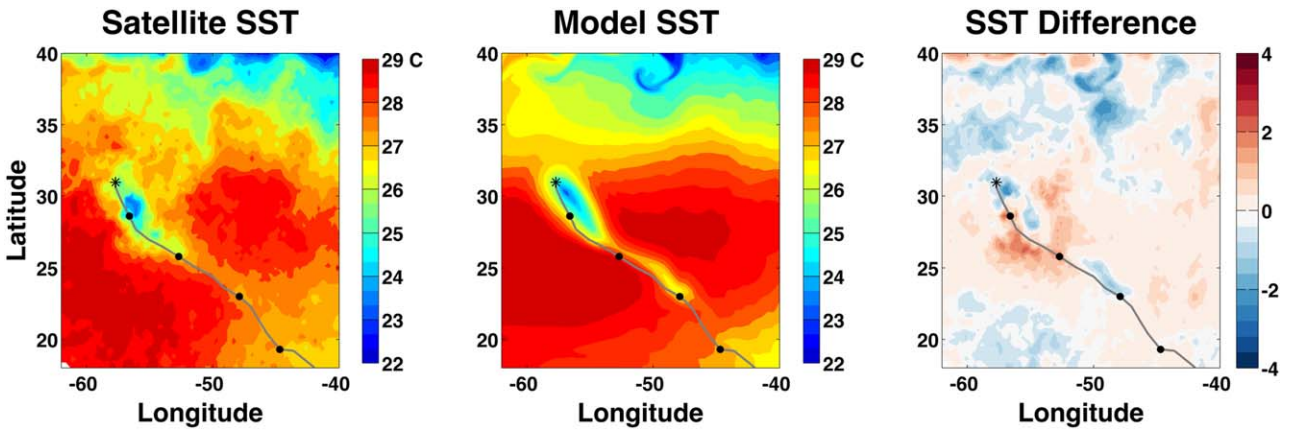

Figure 8. Same as Figure 6 but at 16 September, 1400 UTC. Black dots along storm track are the storm center in 24 hour intervals, at 0000 UTC. The black star marks the storm center at 16 September, 1400 UTC. Only SST results from the KPP-LT model are shown here.

the model temperature horizontally, layer-by-layer, at a series of points along the transect line. Virtual vertical profiles are then made at each point by vertically interpolating onto half-meter depths, and the MLD is found by the above criteria. Similarly the AXBT profile is interpolated onto half-meter depths and, using the above criteria, we find the AXBT MLD.

In summary, the model initialization system produces results that compare well to available observations in terms of both SST and MLD.

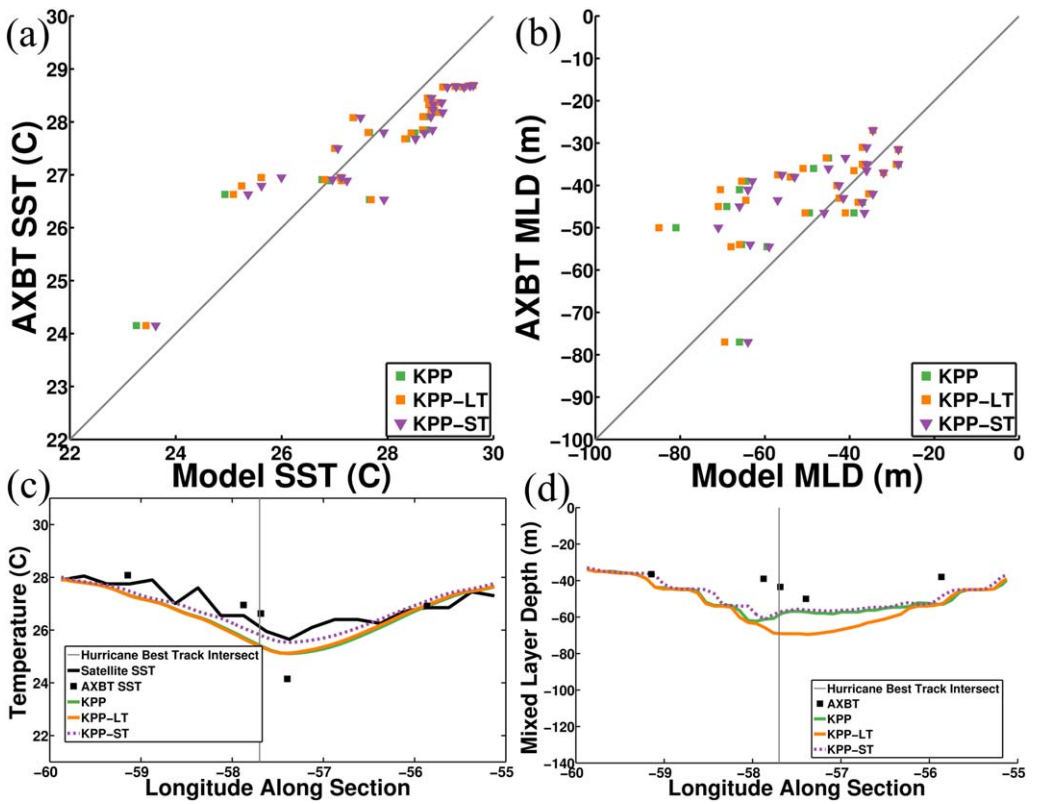

Figure 9. Comparisons between model and observations of SST and mixed layer depth near the storm, from 14 to 16 September. (a) SST, (b) mixed layer depth, (c) SST along Transect B at 16 September, 1400 UTC, (d) mixed layer depth along Transect B at 16 September, 1400 UTC.

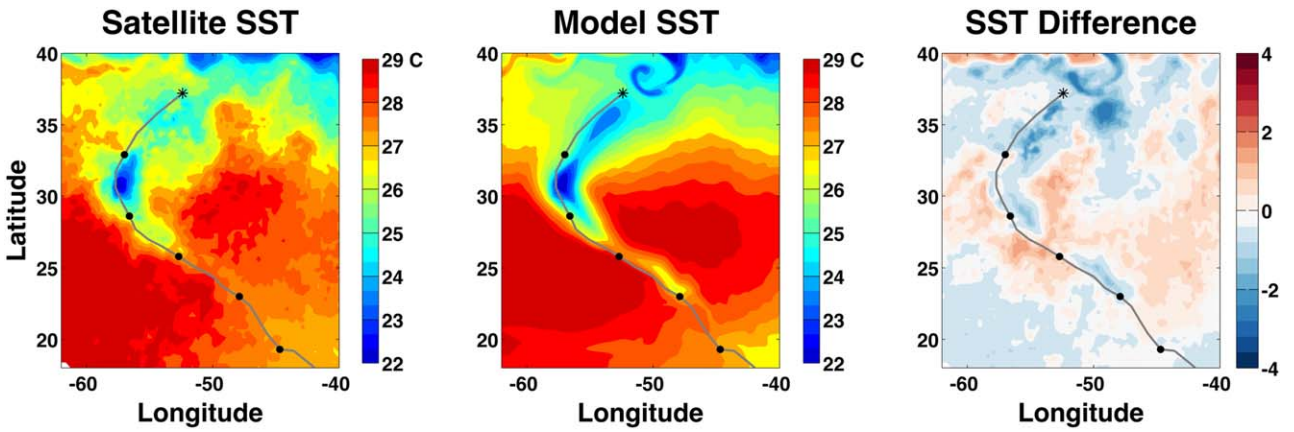

Figure 10. Same as Figure 8 but at 17 September, 1800 UTC. The black star marks the storm center at 17 September, 1800 UTC. Only SST results from the KPP-LT model are shown here.

3.2. Near Storm Conditions

To evaluate the performance of the model near the storm, we examine the results from 14 to 16 September. During this period, the storm strengthened to reach a major hurricane status (Figure 3) and three AXBT deployment flights were performed close to the storm center (Figure 1).

First, the overall SST distribution at 16 September, 1400 UTC is compared between the model result and the satellite observation (Figure 8). Only the model result with the KPP-LT is shown because the model SST difference between KPP and KPP-LT is quite small at this time. Overall, the model accurately predicts the SST cooling behind the storm on the right of the storm track. The model slightly overcool SST just behind the storm center, reaching a maximum difference of approximately 2° C.

The overall agreement between the model results and the AXBT observations during this period is quite satisfactory for both SST and MLD (Figures 9a and 9b). The SST difference is mostly within ± 1° C, and the MLD difference is mostly within ± 10 m for shallower MLD. In the area where the MLD has significantly increased, the model appears to overestimate deepening of the mixed layer. However, we need to be cautious about drawing any conclusions about the model performance, because the results are sensitive to the drag coefficient employed, as discussed later.

At this stage, the model SST values with LT (both KPP and KPP-LT) are consistently lower than those without LT (KPP-ST) by up to 0.5°C. The model SST difference between KPP and KPP-LT is quite small, mostly less

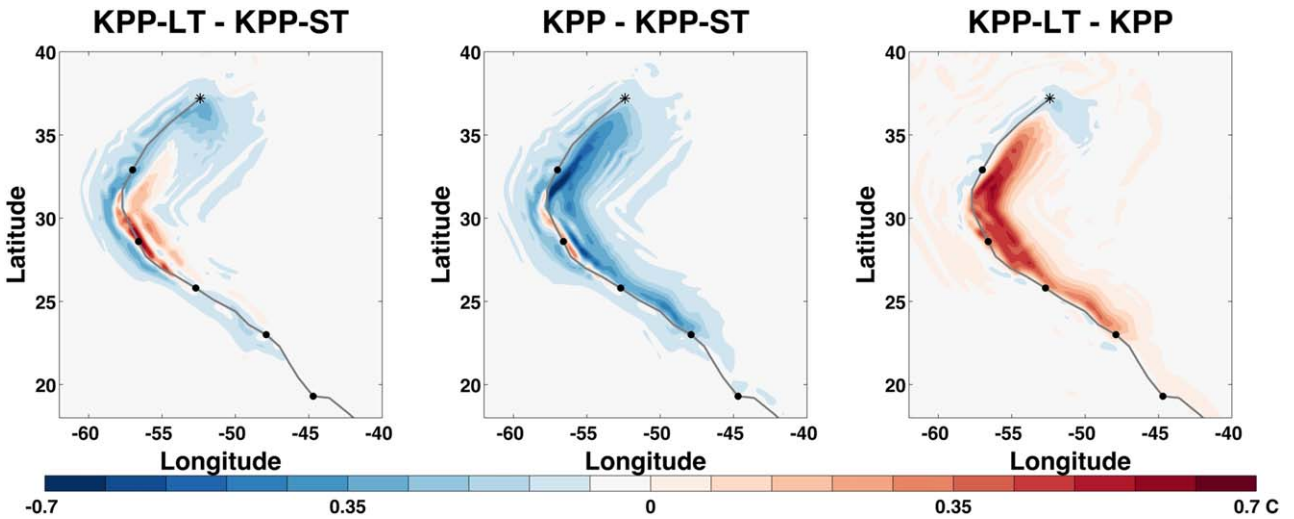

Figure 11. Model differences in SST on 17 September, 1800 UTC. (a) KPP-LT minus KPP-ST, (b) KPP minus KPP-ST, and (c) KPP-LT minus KPP.

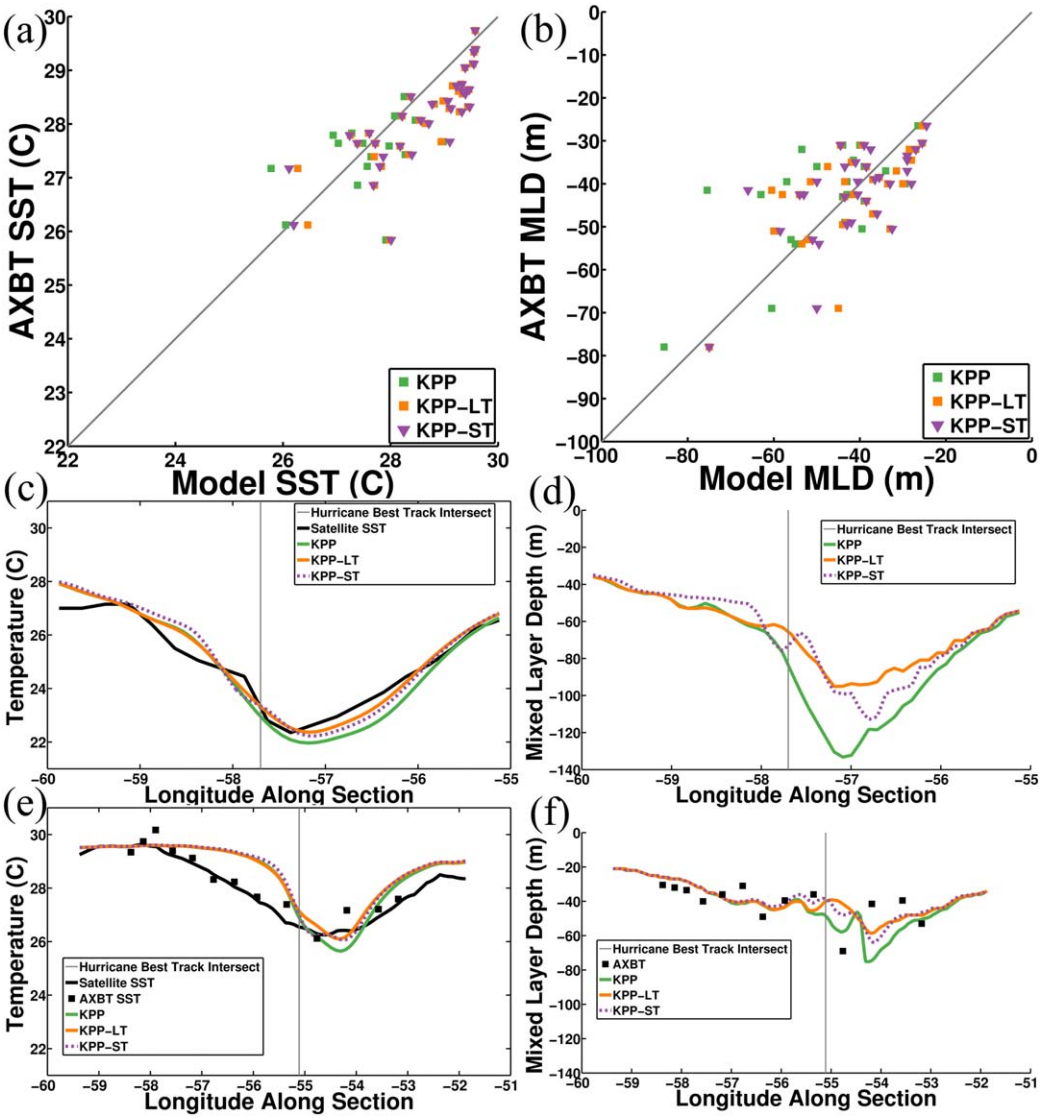

Figure 12. Comparisons between model and observations of SST and mixed layer depth after the storm, at 17 September,1800 UTC. (a) SST, (b) mixed layer depth, (c) SST along Transect B, (d) mixed layer depth along Transect B, (e) SST along Transect A, (f) mixed layer depth along Transect A.

than 0.2°C (Figure 9a). These results suggest that the LT mixing is enhancing the SST cooling, but that the sea state dependence of LT is not appreciably affecting the results. We emphasize here that the SST difference of 0.5°C is not trivial, since SST cooling of this magnitude can reduce the total air-sea heat flux by 10% or more (Reichl et al., 2016b).

The MLD results show more sensitivity to the different mixing schemes (Figure 9b). The KPP MLD is mostly deeper than the KPP-ST MLD, and the KPP-LT MLD is consistently deeper than the KPP MLD, by up to 10–20 m. Therefore, the sea state dependence of LT is affecting the mixed layer deepening.

Next, the model data comparisons are made along Transect B, located very near the storm center and the AXBT drops were made inside the storm (Figure 2). The SST results (Figure 9c) confirm that the SST is not sensitive to the sea state dependence of LT. This figure appears to suggest that the model SST without LT (KPP-ST) agrees better with the observation than those with LT (KPP and KPP-LT). However, we will later show that the KPP-ST result is not better if the drag parameterization based on Sullivan et al. (2012) is used. Therefore, we cannot conclude that the KPP-ST result is more consistent with observations based on Figure 9c alone.

It is interesting that the difference between the KPP-LT MLD and KPP MLD is not uniform, but is more significant near and to the right of the storm track (Figure 9d), where KPP-LT mixed layer is significantly deeper. This is likely because the sea state dependent KPP-LT scheme enhances turbulent mixing corresponding to more developed surface wave fields on the right of the storm track.

3.3. Post Storm Conditions

To examine the model performance after the storm, we use the observations at 17 September, 1800 UTC, where a systematic post storm AXBT survey was conducted (Figure 2).

First, the overall SST fields are compared between the model result (KPP-LT) and the satellite observation (Figure 10). Again, the model produces the cold wake quite accurately, except just behind the storm center where the model underestimates SST. At this time, SST exhibits some sensitivity to different mixing schemes (Figure 11). As expected, KPP, with sea state independent LT, always enhances upper ocean mixing and SST cooling compared to KPP-ST without LT (Figure 11, middle). However, the sea state dependent KPP-LT does not always do so (Figure 11, left). The most notable difference is between KPP-LT and KPP (Figure 11, right). The KPP-LT result predicts significantly warmer SST only to the right of the storm track; SST to the left of the track is very similar between the two mixing schemes. It is interesting to contrast this result to the comparable result obtained using an idealized storm (Figure 13 of Reichl et al. (2016b)), which shows that KPP-LT predicts significantly cooler SST than KPP only to the left of the storm track; both schemes predict similar SST to the right of the storm track. Although these two results are not entirely consistent, they both suggest that the sea state dependent LT effect can be significant and can be quite complex, depending on storm characteristics.

Next, the comparison between the model results and the AXBT observations are shown in Figure 12. Again, the overall agreement is quite satisfactory for both SST and MLD. As discussed above, SST is now dependent on the mixing scheme; KPP consistently predicts lower SST than KPP-LT. It is interesting that the dependence of MLT on the two mixing schemes (KPP and KPP-LT) has almost completely reversed from the earlier near storm results (see Figure 12b compared to Figure 9b); KPP now predicts significantly deeper mixed layer than KPP-LT in many locations. The model results along the two transects also show similar trends, that is, slightly cooler SST and significantly deeper MLD with KPP compared to KPP-LT (Figures 12c–12f).

In summary, the LT can modify the SST cooling by up to 0.5-0.7°C and the MLD by up to 20m. The results with KPP (no sea state dependence) and with KPP-LT (with sea state dependence) can differ by similar magnitudes. These results are quite consistent with the model results by Reichl et al. (2016b) using idealized storms, and confirm the significant LT impact on upper ocean processes under TCs. It is interesting that the KPP-LT results are often closer to the KPP-ST results than the KPP results (see e.g., Figure 12c). However, this does not necessarily mean that the LT effect is weak nor can be neglected in models. When the LT effect is added by simply modifying the critical Richardson number (KPP), the mixed layer deepening and SST cooling are consistently enhanced (mainly 1-D process). When the LT effect is included in more accurate manner including the sea state dependence (KPP-LT), the upper ocean currents and horizontal heat advection are also significantly modified (3-D process) and the LT effect on SST cooling becomes more complex; sometimes the 1-D effect and the 3-D effect cancel each other and make the overall LT impact rather small as discussed by Reichl et al. (2016b).

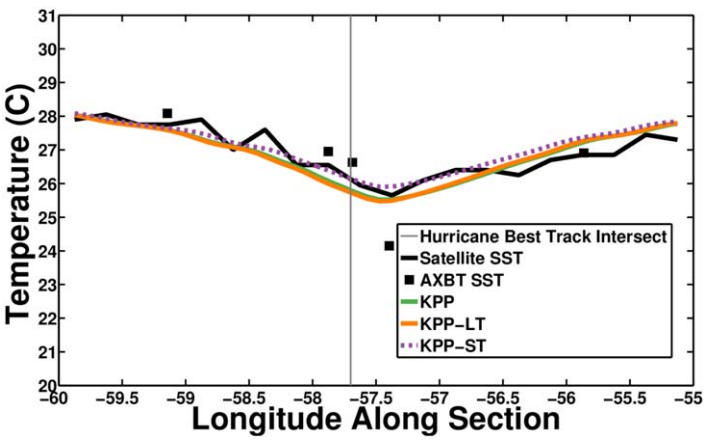

Figure 13. Same as 9c with the Sullivan drag parameterization instead of the HWRF drag parameterization.

It is certainly possible to make more quantitative analysis regarding the agreement between the observations (SST and MLD) and the model results, such as calculating the correlation coefficients and drawing regression lines. However, we have decided not to carry out these calculations because (1) the results can be very different if a different drag coefficient is used as shown in section 3.4, and (2) there are not enough observations to make accurate statistical analyses.

3.4. Dependence on Drag Coefficient Parameterizations

In order to examine the dependence of our model results on different drag coefficient parameterizations, we repeated all experiments with the drag parameterization based on Sullivan et al. (2012). This

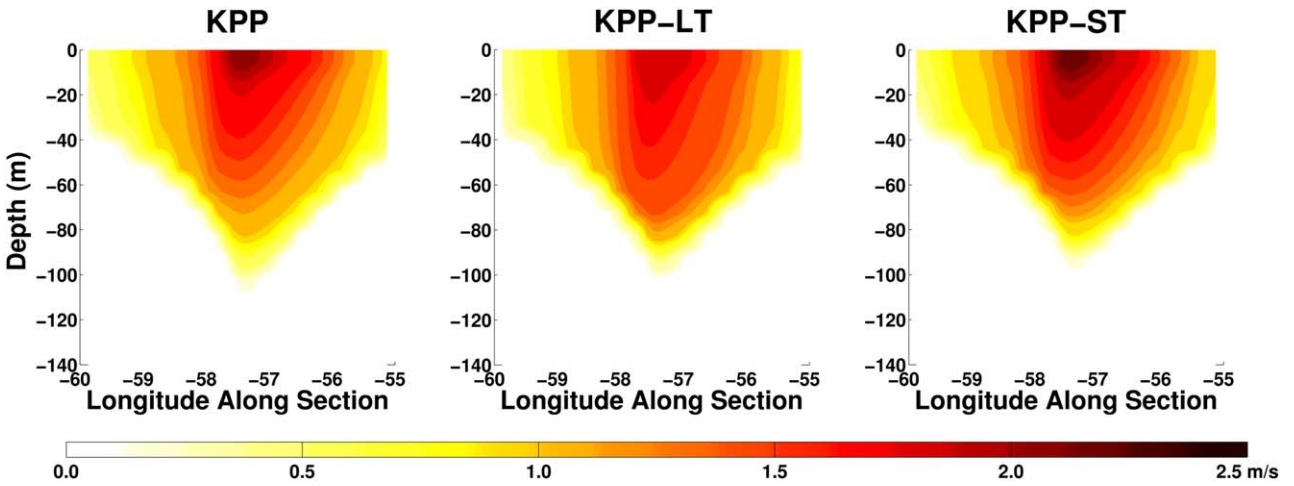

Figure 14. Transect B current magnitude on 16 September, 1400 UTC for (a) KPP, (b) KPP-LT, (c) KPP-ST.

parameterization yields a lower drag coefficient except at very low and very high wind speeds (Figure 5). We have found that the results are systematically similar for all experiments, with only a slight decrease in SST cooling and mixed layer deepening. An example of the SST comparison is shown in Figure 13, where the model SST response and its dependence on different mixing schemes with the Sullivan drag parameterization are very similar to those with the HWRF drag experiments (Figure 9c), but with an overall positive shift in temperature due to the weaker drag.

Because of this dependence of our model results on different drag parameterizations, it is difficult to draw any conclusions regarding whether the sea state dependent KPP-LT is superior to the traditional (sea state independent) KPP or not. Depending on the choice of drag parameterizations the overall model-data agreement can be better with either mixing parameterization. In other words, we may obtain apparently correct model results for the wrong reason if the error in the drag coefficient compensates the error in the mixing scheme. Nevertheless, there are some aspects that suggest KPP-LT might be more accurate than KPP. Figure 12e, f show that KPP-LT yields less asymmetric SST and MLD distributions with respect to the storm track compared to the results with KPP. This trend appears to be more consistent with AXBT observations and does not depend on drag coefficient parameterizations.

3.5. Model Results of Ocean Currents

Reichl et al. (2016b) show that the dependence of the model results on different mixing schemes (KPP and KPP-LT, in particular) is most apparent in near surface current and vertical current shear. They show that the explicit (sea state dependent) LT parameterization typically enhances vertical mixing of momentum, reduces the vertical current shear, and decreases the near surface current magnitude.

Our model results also confirm that upper ocean currents are very sensitive to different mixing schemes. Such an example is shown in Figure 14, where the current magnitude distribution is shown along Transect B near the storm. While both KPP and KPP-ST predict strong surface currents and strong vertical current shear near the storm track, KPP-LT predicts much weaker surface currents and current shear.

4. Conclusions

In this study we have investigated the upper ocean response under Hurricane Edouard using the MPIPOM-TC ocean model with two different mixing schemes, KPP (with sea state independent LT) and KPP-ST (without LT), as well as with a coupled ocean-wave model (MPIPOM-TC and WW3) with the KPP-LT mixing scheme (parameterizing sea state dependent LT). The model results have been compared with the AXBT observations of SST and MLD before, during, and after the storm, as well as satellite SST observations.

Our model results of SST and MLD are generally consistent with the observations. The model quite accurately simulates mixed layer deepening and SST cooling under and behind the storm. The LT can modify

the SST cooling by up to 0.5-0.7°C and the MLD by up to 20m, being consistent with the earlier modeling study using idealized storms (Reichl et al. 2016b). Near the storm, SST is not sensitive to the sea state dependence of the LT, but MLD is slightly enhanced with KPP-LT than with KPP. In post storm conditions after the storm has passed, SST is slightly lower and MLD is significantly enhanced with KPP than with KPP-LT. It is particularly noteworthy that the dependence of MLD on KPP and KPP-LT has reversed from the near storm condition.

When a slightly lower drag coefficient parameterization is introduced, the overall trends of the model results are unchanged but the magnitudes of SST cooling and mixed layer deepening are reduced as expected. Therefore, the overall model-data agreement can be better with either mixing scheme (KPP or KPP-LT), depending on the choice of drag coefficient. This fact, together with the small number of available observations, makes it difficult to draw any conclusion regarding whether the explicit sea state LT parameterization improves the upper ocean model predictions or not. Nevertheless, there are some evidences (e.g., asymmetry of the ocean response with respect to the storm track) that suggest that KPP-LT might be more accurate than KPP.

Both this study and the previous study (Reichl et al., 2016b) show that the difference between the sea state dependent (KPP-LT) and independent (KPP) LT parameterizations is most apparent in upper ocean current and current shear. Therefore, it is desirable to compare model simulations against direct observations of near surface current in order to fully examine the impact of sea state dependent LT under tropical cyclone conditions.

Acknowledgments
The authors acknowledge NOAA/HFIP Grant NA12NWS4680002 and NSF Grants OCE1129985 awarded to the University of Rhode Island and State of Rhode Island for funding this work. Data from cited sources may be obtained per the processes detailed in their respective publications. Further details on model structure or outputs may be obtained at ftp://po.gso.uri.edu/pub/downloads/JGR_Blair_etal.

References

Bender, M., & Ginis, I. (2000). Real-case simulations of hurricane-ocean interaction using a high-resolution coupled model: Effects on hurricane intensity. *Monthly Weather Review*, *128*, 917–946. https://doi.org/10.1175/1520-0493(2000)128<0917:RCSOHO>2.0.CO;2

Bender, M. A., Ginis, I., Tuleya, R., Thomas, B., & Marchok, T. (2007). The operational GFDL coupled hurricane-ocean prediction system and a summary of its performance. *Monthly Weather Review*, *135*, 3965–3989.

Biswas, M. K. L., Bernardet, I., Ginis, Y., Kwon, B., Liu, Q., Liu, T., . . . Zhang, X. (2016). *Hurricane Weather Research and Forecasting (HWRF) model: 2016 Scientific documentation*. Developmental Testbed Center.

Blumberg, A. F., & Mellor, G. L. (1987). A description of a three-dimensional coastal ocean circulation model. In *Three-Dimensional Coastal Ocean Models* (Vol. 4, pp. 1–16). https://doi.org/10.1029/co004p0001

Cione, J. J., Kalina, E. A., Uhlhorn, E. W., Farber, A. M., & Damiano, B. (2016). Coyote unmanned aircraft system observations in Hurricane Edouard (2014). *Earth and Space Science*, *3*, 370–380.

D'Asaro, E., Black, P. G., Centurioni, L., Chang, Y.-T., Chen, S. S., Foster, R., . . . Wu, C.-C. (2014). Impact of typhoons on the ocean in the Pacific: ITOP. *Bulletin of the American Meteorological Society*, *95*, 1405–1418. https://doi.org/10.1175/BAMS-D-12-00104.1

Emanuel, K. (1991). The Theory of hurricanes. *Annual Review of Fluid Mechanics*, *23*, 179–196. https://doi.org/10.1146/annurev.fluid.23.1.179

Falkovich, A., Ginis, I., & Lord, S. (2005). Ocean data assimilation and initialization procedure for the coupled GFDL/URI hurricane prediction system. *Journal of Atmospheric and Oceanic Technology*, *22*, 1918–1932. https://doi.org/10.1175/jtech1810.1

Fan, Y., Ginis, I., & Hara, T. (2010). Momentum flux budget across the air-sea interface under uniform and tropical cyclone winds. *Journal of Physical Oceanography*, *40*, 2221–2242. https://doi.org/10.1175/2010jpo4299.1

Fox-Kemper, B., & Suzuki, N. (2016). Effects of ocean surface gravity waves: On turbulence, climate, and frontogenesis. In *Volume 18 of EGU General Assembly Conference* (Abstracts 2281). Munich, Germany: European Geosciences Union.

Ginis, I. (2002). Tropical cyclone-ocean interactions. *Advances in Fluid Mechanics*, *33*, 83–114.

Halliwell, G. R., Shay, L. K., Jacob, S. D., Smedstad, O. M., & Uhlhorn, E. W. (2008). Improving ocean model initialization for coupled tropical cyclone forecast models using GODAE nowcasts. *Monthly Weather Review*, *136*, 2576–2591.

Jaimes, B., Shay, L. K., & Uhlhorn, E. (2015). Enthalpy and momentum fluxes during Hurricane Earl. relative to underlying ocean features. *Monthly Weather Review*, *143*, 111–131.

Large, W. G., McWilliams, J. C., & Doney, S. C. (1994). Oceanic vertical mixing: A review and a model with a nonlocal boundary layer parameterization. *Reviews of Geophysics*, *32*, 363–403. https://doi.org/10.1029/94RG01872

Lin, I.-I., Black, P., Price, J. F., Yang, C.-Y., Chen, S. S., Lien, C.-C., . . . D'asaro, E. A. (2013). An ocean coupling potential intensity index for tropical cyclones. *Geophysical Research Letters*, *40*, 1878–1882. https://doi.org/10.1002/grl.50091

Mellor, G. (2004). Users guide for a three–dimensional, primitive equation numerical ocean model, available on the Princeton Ocean Model (POM) website, rev. 2004.

Mellor, G. L., & Yamada, T. (1982). Development of a turbulence closure model for geophysical fluid problem. *Reviews of Geophysics*, *20*, 851–875. https://doi.org/10.1029/RG020i004p00851

Rabe, T. J., Kukulka, T., Ginis, I., Hara, T., Reichl, B. G., D'Asaro, E. A., . . . P. P. Sullivan (2015). Langmuir turbulence under Hurricane Gustav (2008). *Journal of Physical Oceanography*, *45*(3), 657–677. https://doi.org/10.1175/jpo-d-14-0030.1

Reichl, B. G., Ginis, I., Hara, T., Thomas, B., Kukulka, T., & Wang, D. (2016a). Impact of sea state dependent Langmuir turbulence on the ocean response to a tropical cyclone. *Journal of Physical Oceanography*. https://doi.org/10.1175/mwr-d-16-0074.1

Reichl, B. G., Wang, D., Hara, T., Ginis, I., & Kukulka, T. (2016b). Langmuir Turbulence Parameterization in Tropical Cyclone Conditions. *Journal of Physical Oceanography*. https://doi.org/10.1175/jpo-d-15-0106.1

Reynolds, R. W., & Smith, T. M. (1994). Improved global sea surface temperature analyses using optimum interpolation. *Journal of Climate*, *7*, 929–948.

Schade, L. R., & Emanuel, K. A. (1999). The ocean's effect on the intensity of tropical cyclones: Results from a simple coupled atmosphere-ocean model. *Journal of the Atmospheric Sciences*, *56*, 642–651.

Smith, J. A. (2006). Wave-Current Interactions in Finite Depth. *Journal of Physical Oceanography*, *36*, 1403–1419. https://doi.org/10.1175/jpo2911.1

Stewart, S. R. (2014). *Tropical cyclone report: Hurricane Edouard*. Miami, FL: National Hurricane Center.

Sullivan, P. P., Romero, L., McWilliams, J. C., & Melville, W. K. (2012). Transient evolution of Langmuir turbulence in ocean boundary layers driven by hurricane winds and waves. *Journal of Physical Oceanography*, *42*(11), 1959–1980. https://doi.org/10.1175/jpo-d-12-025.1

Teague, W. J., Carron, M. J., & Hogan, P. J. (1990). A comparison between the Generalized Digital Environmental Model and Levitus Climatologies. *Journal of Geophysical Research*, *95*, 7167–7183.

Tolman, H. L. (2009). User manual and system documentation of WAVEWATCH III TM version 3.14. Technical note, MMAB Contribution.

Trahan, S., & Sparling, L. (2012). An analysis of NCEP tropical cyclone vitals and potential effects on forecasting models. *Weather Forecasting*, *27*, 744–756. https://doi.org/10.1175/WAF-D-11-00063.1.

Yablonsky, R. M., & Ginis, I. (2008). Improving the ocean initialization of coupled hurricane ocean models using feature-based data assimilation. *Monthly Weather Review*, *136*, 2592–2607. https://doi.org/10.1175/2007mwr2166.1

Yablonsky, R. M., & Ginis, I. (2009). Limitation of one-dimensional ocean models for coupled hurricane ocean model forecasts. *Monthly Weather Review*, *137*, 4410–4419. https://doi.org/10.1175/2009mwr2863.1

Yablonsky, R. M., Ginis, I., & Thomas, B. (2015a). Ocean modeling with flexible initialization for improved coupled tropical cyclone-ocean model prediction. *Environmental Modelling & Software*, *67*, 26–30. https://doi.org/10.1016/j.envsoft.2015.01.003

Yablonsky, R. M., Ginis, I., Thomas, B., Tallapragada, V., Sheinin, D., & Bernardet, L. (2015b). Description and analysis of the ocean component of NOAA's operational Hurricane Weather Research and Forecasting (HWRF) Model. *Journal of Atmospheric and Oceanic Technology*, *32*, 144–163.

Zhang, J. A., Cione, J. J., Kalina, E. A., Uhlhorn, E. W., Hock, T., & Smith, J. A. (2017). Infrared sea surface temperature measurements from Hurricane Edouard (2014) using GPS dropsondes. *Journal of Atmospheric and Oceanic Technology*, *34*, 1333–1349.